PAPER

Check for updates

Benzimidazole–dioxoisoindoline conjugates as dual VEGFR-2 and FGFR-1 inhibitors: design, synthesis, biological investigation, molecular docking studies and ADME predictions†

Heba T. Abdel-Mohsen [ID] *[a] and Amira M. Nageeb[b]

In this investigation, a new series of benzimidazole–dioxo(benzo)isoindoline hybrids **8a–o** were rationally designed and synthesized. All the synthesized hits **8a–o** were investigated for their VEGFR-2 inhibitory activity at 10 μM. The conjugates **8l** and **8m** demonstrated potent inhibitory activity of 87.61 and 80.69%, respectively. Further evaluation of **8l** and **8m** on FGFR-1 at 10 μM demonstrated % inhibition = 84.20 and 76.83%, respectively. Investigation of the growth inhibitory activity of the synthesized hits on NCI cancer cell lines showed that the benzimidazole–dioxobenzoisoindoline hybrid **8m** exhibits the highest antiproliferative activity. It displayed growth inhibitory activity reaching 89.75%. Examination of the effect of **8m** on the cell cycle of MCF7 cell line revealed its ability to induce arrest of the cell cycle at the G2/M phase and its potential to induce the apoptosis of the same cell line. Additionally, the benzimidazole–dioxobenzoisoindoline hybrid **8m** had potent anti-migratory properties as evidenced by the delay in the wound closure in reference to untreated control cells. Molecular docking of **8m** in the binding pockets of the VEGFR-2 and FGFR-1 proved its ability to occupy the binding pockets of both targets in type II inhibitor binding mode and to perform the essential interactions with the crucial amino acids in the binding pockets of both targets. Moreover, ADME prediction studies demonstrated the drug like properties of the synthesized benzimidazole–dioxoisoindolines **8a–o**.

1. Introduction

Each year, more and more people are diagnosed with cancer,[1] which presents a problem for world health.[1,2] Genetic changes and/or overexpression of certain protein kinases (PKs) are linked to many cancer forms.[3,4] As a result, PKs have therefore received a lot of interest recently as potential biological targets for the discovery of new tailored medications for the prevention and control of cancer progression.[3–8]

Numerous studies have reported a link between the pathophysiology of cancer and the development of new blood vessels (angiogenesis)[6,9] which is necessary for the growth and dissemination of cancer by supplying it with nutrients and removing waste. Thus, a popular strategy for treating cancer is to target the protein kinases that start and maintain the angiogenic process.[10] A tyrosine kinase system called vascular

endothelial growth factor (VEGF) and its receptors (VEGFRs) play a critical role in angiogenesis in both healthy and pathological circumstances.[10–12] In contrast to healthy tissues, VEGFR-2 is overexpressed in a number of cancer types.[13,14] Additionally, the FGFR family is a group of four isoforms, FGFR-1 to FGFR-4, that are expressed on the cell membrane and take part in a number of critical physiological and pathological processes, including angiogenesis, cell migration and survival.[15] Different forms of solid tumors have been shown to overexpress FGFRs.[16] Therefore, it is thought that inhibiting FGFRs using small molecules is an appealing strategy for the development of innovative anticancer agent.[17–20]

As time went on, researchers became interested in benzimidazoles as a scaffolding core that could be customized for the creation of new chemotherapeutic agents.[19–24] For example, the protein data bank shows the crystal structure of the benzimidazole derivative **I** (PDB ID: 2QU5) (Fig. 1 and 2) in the active pocket of VEGFR-2. It demonstrated a K_i of 8.7 nM against VEGFR-2.[25] Masaichi Hasegawa *et al.* revealed a novel series of benzimidazole–ureas as inhibitors of VEGFR-2. The derivative **II** showed IC$_{50}$ = 3.5 nM and its crystal structure in the active site of VEGFR-2 is depicted in the PDB under the ID: 2OH4.[26] Dovitinib (**III**), a multi-kinase inhibitor that inhibits VEGFR1-3, FGFR1-3, and PDGFR, has also been used to treat a number of

[a]Chemistry of Natural and Microbial Products Department, Pharmaceutical and Drug Industries Research Institute, National Research Centre, Dokki, P.O. 12622, Cairo, Egypt. E-mail: hebabdelmohsen@gmail.com; ht.abdel-mohsen@nrc.sci.eg

[b]High Throughput Molecular and Genetic Technology Lab, Center of Excellence for Advanced Sciences, Biochemistry Department, Biotechnology Research Institute, National Research Centre, Dokki, P.O. 12622, Cairo, Egypt

tumor types, including renal cell carcinoma, gastrointestinal stromal tumors, colorectal cancer, and ovarian cancer.[27,28] The X-ray crystal structure of Dovintib with the FGFR-1 active site was reported by Bunney, T. *et al.* (PDB ID: 5AM6).[29] Additionally, melanoma and colorectal cancer were found to be sensitive to the dual BRAF/VEGFR-2 inhibitor RAF265 (**IV**) (PDB ID: 5CT7)[30] (Fig. 1).

Recently, our research group have identified the essential pharmacophoric features of type II VEGFR-2, FGFR-1 and BRAF inhibitors.[19] Taking the crystal structure of the benzimidazole derivative **I** in the binding site of VEGFR-2 (PDB ID: 2QU5) as an example,[25] the derivative binds to the inactive form of VEGFR-2 in type II inhibitors binding mode. The pyridine moiety occupies the hinge region where it is involved in hydrogen bonding, through the nitrogen of the pyridine and the carboxamide NH, with Cys919, while fused benzene ring of the benzimidazole system acts as a spacer enabling the 2-amino-imidazole moiety to be involved through one of the two N–H groups and C=N group in hydrogen bonding with Glu885 and Asp1046, respectively, while the phenyl group at the two position is settled in hydrophobic back pocket forming hydrophobic interactions with the amino acids lining this pocket (Fig. 2).

In reference to the identified essential fragments on one hand[19] and the binding mode of the benzimidazole derivative **I** in the VEGFR-2's active site on the other hand,[25] we have reported a new series of 2,5-diaryl benzimidazoles of potent activity on diverse kinases. Compound **V** is a representative example from the series and it showed IC$_{50}$ values of 0.93, 3.74, 0.25 μM, against VEGFR-2, FGFR-1 and BRAF, respectively. Additionally, potential activity on NCI cancer cell lines was detected with GI$_{50}$ up to 0.66 μM.[19]

As a continuation of our previous work, the present approach aims at replacement of the benzylidene moiety of compound **V** with dioxo(benzo)isoindoline moiety for the design of a new class of benzimidazole–dioxo(benzo)isoindoline conjugates of the general structure **VI** (Fig. 2) as type II VEGFR-2 and FGFR-1

inhibitors. The design approach considers that the benzimidazole nucleus's NH group will remain free such that the benzimidazole would be settled in target kinases' gate area and are expected to be stabilized by the engagement of the NH and C=N groups through hydrogen bonding with Glu885 and Asp1046 of VEGFR-2's, and Glu531 and Asp641 of FGFR-1's binding pockets, respectively. Additionally, the 5-position would be functionalized by the inclusion of a dioxo(benzo)isoindoline moieties to fit in the hinge region of the target kinases where the carbonyl group would participate in hydrogen bonding with the key amino acids Cys919 (VEGFR-2) and Ala564 (FGFR-1) in the hinge region. In the meantime, the two position of the benzimidazole scaffold would be decorated with hydrophobic aryl moieties to be directed toward the hydrophobic back pocket of the target kinases (Fig. 2).

After the proposed compounds are synthesized, their inhibitory activity on VEGFR-2 will be evaluated. Next, the inhibitory potency of the most potent candidate on FGFR-1 would be evaluated. In parallel, each of the synthesized candidates would be evaluated for its ability to inhibit the growth of various cancer cell lines. The most effective derivative would next be examined for its effects on the cell cycle and apoptosis of a selected cancer cell line. Additionally, a wound healing assay would be employed to further demonstrate the antiangiogenic ability of the most potent candidate. Moreover, molecular docking of the most effective candidate on the target kinases would be carried out to prove the design strategy.[31] Ultimately, the submission of the synthesized derivatives to the SwissADME webtool would forecast their physicochemical features.[32]

2. Results and discussion

2.1. Chemistry

The initial 2-substituted-benzimidzole-5-carboxylic acids **4a–e** were prepared by reacting the benzoic acid derivative **3** with different aryl aldehyde sodium bisulfite adducts **2a–e**. Then,
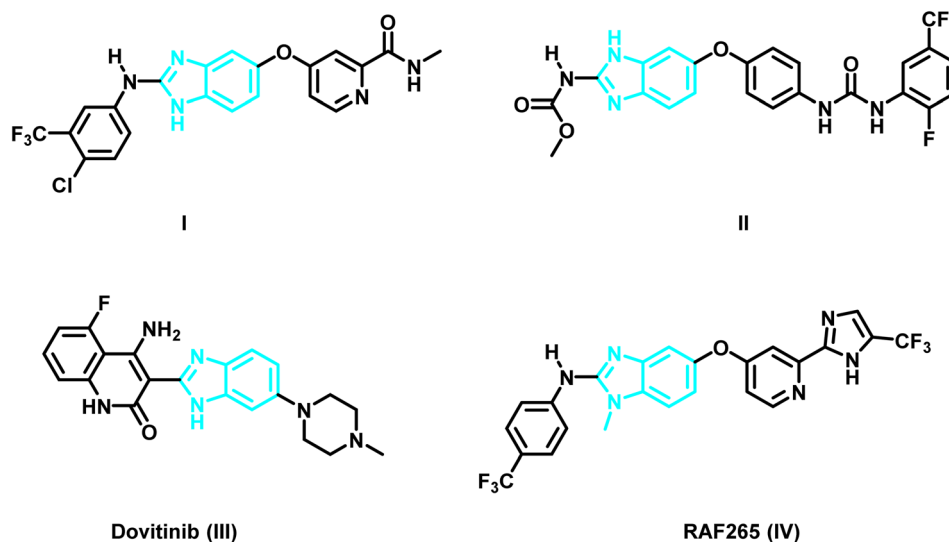

Fig. 1 Benzimidazole-based multi-kinase inhibitors.
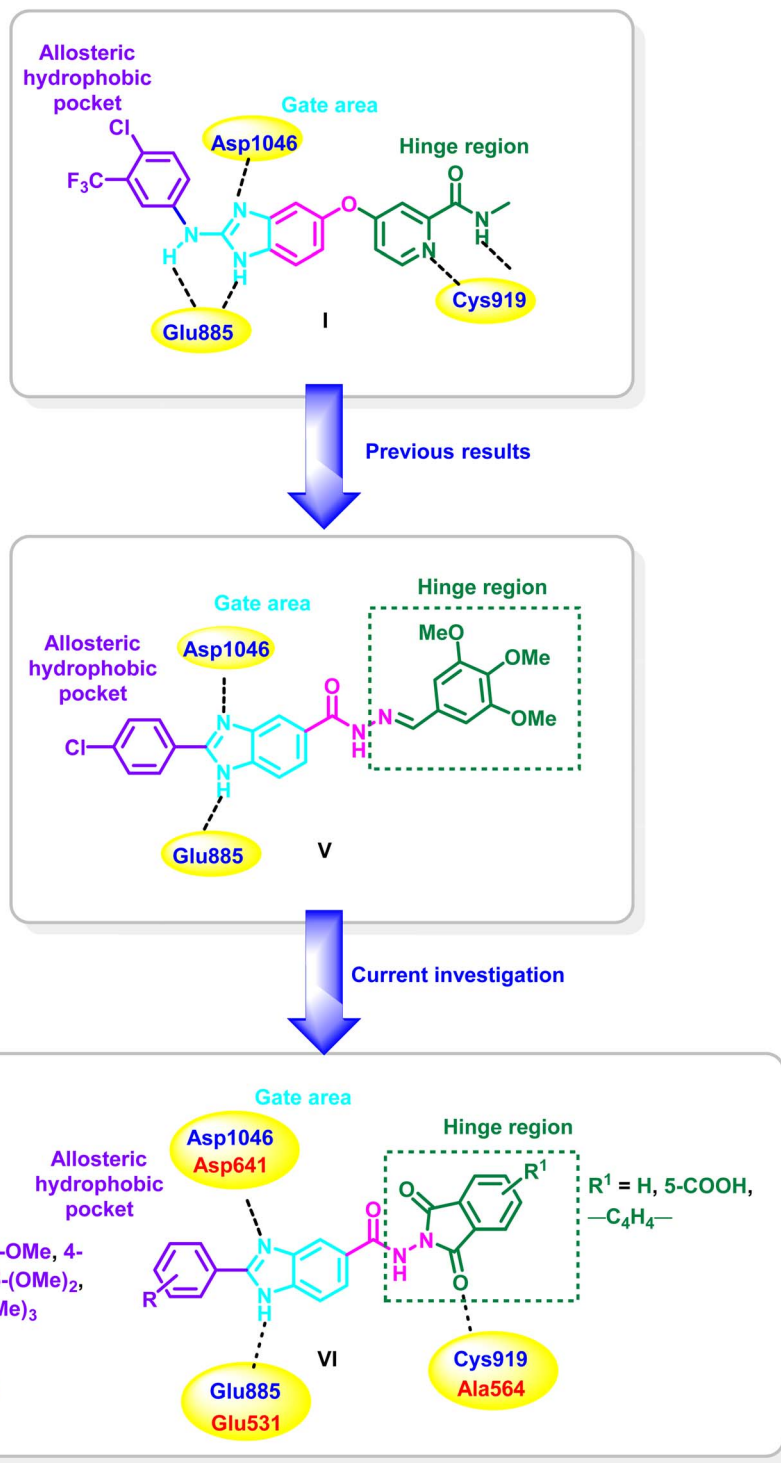
Fig. 2 Suggested strategy for the design of benzimidazole–dioxo(benzo)isoindoline conjugates **VI**.

through a reaction with ethanol in the presence of sulfuric acid, the benzimidazole derivatives **4a–e** were transformed into the ester congeners **5a–e**. The reaction of **5a–e** with hydrazine hydrate produced the hydrazide derivatives **6a–e**. Finally, the hydrazides **6a–e** and acid anhydrides **7a–c** were allowed to react in acetic acid to produce the target hybrids **8a–o** (Scheme 1).

2.2. Biology

2.2.1. Biochemical assay

2.2.1.1 VEGFR-2 inhibitory activity. The capacity to inhibit VEGFR-2 at a concentration of 10 μM was tested for the designed and synthesized 2-(substituted)-*N*-(1,3-

1,2,4,5,6a R = Cl
1,2,4,5,6b R = 3-OMe
1,2,4,5,6c R = 4-OMe
1,2,4,5,6d R = 2,5-(OMe)$_2$
1,2,4,5,6e R = 3,4,5-(OMe)$_3$

7a R^1 = H
7b R^1 = COOH

8a–j

8a R = 4-Cl, R^1 = H
8b R = 3-OMe, R^1 = H
8c R = 4-OMe, R^1 = H
8d R = 2,5-(OMe)$_2$, R^1 = H
8e R = 3,4,5-(OMe)$_3$, R^1 = H

8f R = 4-Cl, R^1 = COOH
8g R = 3-OMe, R^1 = COOH
8h R = 4-OMe, R^1 = COOH
8i R = 2,5-(OMe)$_2$, R^1 = COOH
8j R = 3,4,5-(OMe)$_3$, R^1 = COOH

8k–o

8k R = 4-Cl
8l R = 3-OMe
8m R = 4-OMe
8n R = 2,5-(OMe)$_2$
8o R = 3,4,5-(OMe)$_3$

Reagents and condition: (i) Na$_2$S$_2$O$_5$, H$_2$O, MeOH, r.t; (ii) DMF, reflux, 3h; (iii) H$_2$SO$_4$, EtOH, reflux, 8h; (iv) NH$_2$-NH$_2$.H$_2$O, EtOH, reflux, 5h; (v) glacial acetic acid, reflux, 3h

Scheme 1 Pathway for the synthesis of the benzimidazole–dioxo(benzo)isoindolines **8a–o**.

dioxoisoindolin-2-yl)-1*H*-benzo[*d*]imidazole-5-carboxamide **8a–o**, sorafenib and the findings are shown in Table 1.

The nature of the substituents on the 2-aryl moiety of the benzimidazole core as well as on the dioxoisoindole moiety has a considerable impact on the degree of VEGFR-2 inhibition. In series **8a–e**, the 4-methoxyphenyl-benzimidazole derivative **8c** displayed the most potent inhibitory activity with % inhibition = 71.11% (Table 1 and Fig. 3).

Moderate inhibitory activity on VEGFR-2 was observed when the 4-methoxyphenyl group was replaced with 3-

methoxyphenyl, 2,5-dimethoxyphenyl or 3,4,5-trimethoxyphenyl moiety in **8b**, **8d** and **8e**, respectively (% inhibition = 37.94–48.90%). On the other hand, the inhibitory action was drastically reduced when the 4-methoxyphenyl group in **8c** was replaced with the 4-chlorophenyl group in **8a** (71.11% inhibition in **8c** *versus* 5.23% inhibition in **8a**, respectively) (Table 1 and Fig. 3).

Introduction of a carboxylic group at the 5-position of the dioxoisoindoline moiety to yield series **8f–j** resulted in increasing the potency for **8f** (% inhibition = 53.54%) and **8g** (%

Table 1 Percentage inhibition of VEGFR-2 after treatment with 10 μM of **8a–o** in comparison to sorafenib

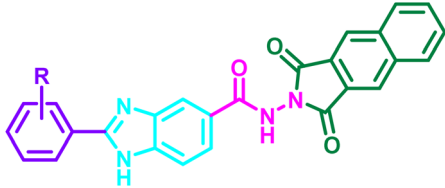| Compound ID	R	R^1	% Inhibition
8a	4-Cl	H	5.23 ± 0.37
8b	3-OMe	H	37.94 ± 2.92
8c	4-OMe	H	71.11 ± 5.63
8d	2,5-(OMe)$_2$	H	43.48 ± 3.38
8e	3,4,5-(OMe)$_3$	H	48.90 ± 4.14
8f	4-Cl	COOH	53.54 ± 5.04
8g	3-OMe	COOH	60.37 ± 5.57
8h	4-OMe	COOH	34.54 ± 2.36
8i	2,5-(OMe)$_2$	COOH	24.87 ± 2.19
8j	3,4,5-(OMe)$_3$	COOH	38.56 ± 2.25
8k	4-Cl	—	21.16 ± 1.96
8l	3-OMe	—	87.61 ± 5.68
8m	4-OMe	—	80.69 ± 6.43
8n	2,5-(OMe)$_2$	—	47.19 ± 3.56
8o	3,4,5-(OMe)$_3$	—	9.87 ± 0.85
Sorafenib			99.63 ± 7.89
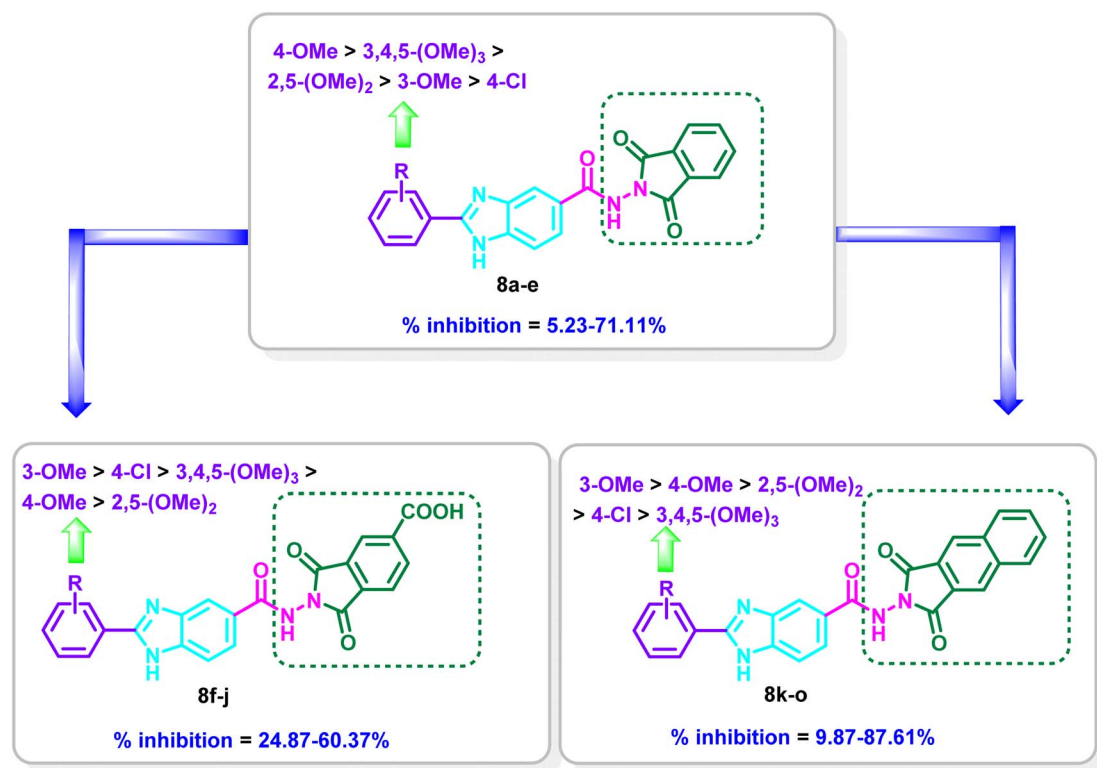
Fig. 3 Structure–activity relationship of the benzimidazoles–dioxo(benzo)isoindoline conjugates **8a–o** on the inhibition percentage of VEGFR-2.

Table 2 % Inhibition of VEGFR-2 and FGFR-1 after treatment with 10 μM of **8l**, **8m** and sorafenib

Compound ID	R	% Inhibition of VEGFR-2	% Inhibition of FGFR-1
8l	3-OMe	87.61 ± 5.18	84.20 ± 7.43
8m	4-OMe	80.69 ± 6.41	76.83 ± 5.06
Sorafenib	—	99.63 ± 7.89	92.37 ± 3.84

inhibition = 60.36%) in reference to **8a** (% inhibition = 5.23%) and **8b** (% inhibition = 37.94%), while a decrease in the potency was observed for **8h–j** (% inhibition = 24.87–38.56%) in comparison to **8c–e** (% inhibition = 43.48–71.11%). In series **8f–j**, compound **8g** incorporating 3-methoxyphenyl moiety displayed the most potent inhibitory activity (% inhibition = 60.37%). Meanwhile, the 4-chlorophenyl derivative **8f**, the 4-methoxyphenyl derivative **8h**, 2,5-dimethoxyphenyl **8i** and 3,4,5-trimethoxyphenyl derivative **8j** showed reduction in potency (% inhibition = 24.87–53.54%) (Table 1 and Fig. 3).

Replacement of 1,3-dioxoisoindolin-2-yl in series **8a–e** with 1,3-dioxo-1,3-dihydro-2H-benzo[f]isoindol-2-yl in series **8k–o** resulted mainly in increasing the % inhibition. The derivative **8o** is the only exception where a decrease in the potency was found relative to **8e** (% inhibition = 9.87% in **8o** versus 48.90% in **8e**). Compound **8l** displayed the most potent activity on VEGFR-2 with % inhibition = 87.61%. Shifting of the 3-methoxy group to the 4-position to give **8m** revealed a slight decrease in the inhibitory activity (inhibition % = 80.69%), while the 2,5-dimethoxyphenyl derivative **8n** displayed moderate activity of 47.19% and the 3,4,5-trimethoxyphenyl derivative **8o** revealed weak % inhibition of 9.87% (Table 1 and Fig. 3).

2.2.1.2 Determination of inhibitory activity of 8l and 8m on FGFR-1. Compounds **8l**, **8m** and sorafenib where further analysed for their inhibitory activity on FGFR-1 at 10 μM and the % inhibition where depicted in Table 2.

The benzimidazole–dioxobenzoisoindolines **8l** and **8m** demonstrated promising inhibitory activity on FGFR-1 with % inhibition = 84.20 and 76.83%, respectively. It is obvious that compound **8l** demonstrated slight better inhibitory activity on VEGFR-2 and FGFR-1 over **8m**.

2.2.2. Cellular assays

2.2.2.1 Antiproliferative activity. The capacity of each target benzo[d]imidazole-1,3-dioxoisoindoline hybrids **8a–o** to suppress the growth of NCI 60 cancer cell lines at 10 μM concentration was tested at NCI, and the findings are shown in Table 3.

The synthesized hybrids **8a–o** demonstrated mild to strong inhibitory effects on a variety of cancer types. According to Table 3, compound **8m** exhibits mainly a moderate to strong GI% against the examined cell lines. It has GI% greater than 50%

against the leukemia cell lines HL-60(TB), K-562, MOL-4, and SR. NCI-H460 cell line from non-small cell lung cancer and SF-539 from CNS cancer are additionally sensitive to **8m**. Furthermore, **8m** showed moderate to strong activity on the melanoma cell lines LOX IMVIL, MDA-MB-435, and SK-MEL-5 with GI% = 51.38, 89.75 and 58.49%, respectively. Furthermore, it had strong action (GI% > 60%) against OVCAR-3 and RXF 393 from ovarian and renal carcinoma, respectively. On MCF7 and MDA-MB-468 breast cancer cell lines, **8m** also showed strong inhibitory action with GI% = 72.06 and 69.10%, respectively (Table 3). Based on the results presented in Table 3, we can conclude that cell lines derived from leukemia, melanoma and breast cancer are the most sensitive to **8m**.

2.2.2.2 Evaluation of the cytotoxic activity of 8m on MCF-7 cell line. Encouraged by the potent activity of **8m** on diverse NCI cancer cell lines, **8m** was further assayed for its growth inhibitory activity on MCF-7 cell line using SRB assay[33] and the IC_{50} was depicted in Table 4. It was found that **8m** showed potent IC_{50} of 5.03 μM in reference to sorafenib which showed IC_{50} = 3.24 μM.

2.2.2.3 Cell cycle analysis. The MCF-7 cell line's cell cycle progression was tested using the representative benzimidazole–dioxobenzoisoindoline derivative **8m** at 5.0 μM concentration. Fig. 4 and Table 5 shows the findings of breast cancer MCF-7 cells before and after treatment with **8m**. After treatment, the proportion of MCF-7 cells that had accumulated in the G1 phase dropped from 57.89 to 51.04%. Contrarily, the total proportion of cells in the G2/M phase rose from 18.23% to 25.26%. These findings show that **8m** causes the division of MCF-7 cell line to stop at the G2/M phase. Additionally, due to cell death, there was a slight elevation in the percentage of cells that accumulated in the sub-G1 phase, going from 1.63% in the control cells to 2.08% in the **8m** treated cells.

2.2.2.4 Apoptosis assay. The potential of **8m** to stimulate the apoptosis of MCF-7 cell line at 5 and 10 μM (Fig. 5) was investigated. According to the findings, at 5 μM, **8m** showed a slight elevation of the percentage of cells in the early and late apoptosis stages (0.28 and 0.99%, respectively) as well as in the necrosis stage (2.00%) in reference to untreated cells. At 10 μM, **8m** potentiate the early and late apoptosis as the percentage of

Table 3 NCI 60 cancer cell line panel's *in vitro* growth inhibition percentage (GI%) following treatment with 10 µM of the benzimidazole–dioxoisoindoline hybrids **8a–o**

Cell line	8a	8b	8c	8d	8e	8f	8g	8h	8i	8j	8k	8l	8m	8n	8o
Leukaemia															
CCRF-CEM	8.31	4.56	—[a]	5.49	—	—	—	16.52	4.00	—	34.48	21.28	45.83	23.52	5.97
HL-60(TB)	—	11.16	—	4.67	14.40	—	6.30	14.05	0.13	11.13	7.15	17.62	54.16	—	7.12
K-562	11.40	9.03	3.99	5.26	3.22	—	3.90	3.13	—	—	7.72	10.61	55.96	5.51	4.09
MOLT-4	0.17	4.97	7.00	—	6.94	—	—	0.82	5.04	4.70	27.46	27.04	75.51	5.04	10.84
RPMI-8226	6.77	5.32	1.28	6.77	—	2.62	1.15	9.54	8.29	—	45.06	41.00	32.35	7.78	13.64
SR	18.06	22.26	nd[b]	8.63	26.01	nd	11.56	16.30	6.50	23.39	nd	nd	61.77	nd	nd
Non-small cell lung cancer															
A549/ATCC	5.59	1.51	—	9.11	5.20	—	—	3.13	5.73	11.81	21.23	—	40.46	—	3.02
EKVX	13.33	4.13	—	10.43	—	4.11	1.71	0.72	6.38	6.40	0.60	0.21	13.77	—	2.63
HOP-62	6.21	4.22	—	0.18	0.17	—	—	—	1.63	4.66	—	—	25.04	7.00	1.40
HOP-92	—	—	—	2.01	—	—	—	17.03	1.51	0.40	—	—	—	3.75	—
NCI-H226	10.20	—	—	3.78	—	—	—	16.02	4.32	—	7.71	1.96	21.07	—	—
NCI-H23	10.05	0.67	1.28	3.23	—	1.71	—	0.49	—	—	1.64	4.46	20.56	1.15	2.27
NCI-H322M	0.39	2.08	—	3.29	5.92	—	—	—	—	1.10	—	3.95	nd	—	—
NCI-H460	8.80	—	—	—	—	—	—	—	—	—	12.76	2.16	52.04	—	—
NCI-H522	12.03	7.22	5.00	11.56	3.79	0.83	6.58	7.54	9.35	5.68	5.96	6.63	25.52	7.41	—
Colon cancer															
COLO 205	—	—	—	—	—	—	—	—	—	—	—	—	11.29	1.62	—
HCC-2998	—	—	—	—	—	—	—	—	—	—	—	1.26	—	—	—
HCT-116	12.07	—	—	—	—	—	—	0.17	—	—	5.85	—	30.91	3.56	—
HCT-15	9.99	5.11	1.92	1.06	5.00	—	—	—	3.67	0.04	7.15	10.36	44.24	—	1.86
HT29	5.42	—	—	7.25	—	—	—	0.49	0.57	3.24	4.90	0.12	39.62	1.29	—
KM12	—	—	—	—	—	—	—	—	—	—	—	7.80	16.31	3.35	—
SW-620	5.76	—	—	4.35	nd	—	—	—	3.04	nd	—	—	19.15	—	—
CNS cancer															
SF-268	1.96	—	—	1.79	—	—	—	—	0.28	—	—	1.55	24.65	—	—
SF-295	16.71	8.43	—	4.43	—	1.00	—	0.34	7.93	8.17	19.28	21.59	37.80	0.56	—
SF-539	12.81	5.54	—	1.70	—	—	—	1.83	0.27	2.75	34.04	31.92	55.89	13.55	6.46
SNB-19	nd	9.50	—	nd	1.58	—	0.20	nd	nd	4.55	18.95	14.83	25.73	3.45	—
SNB-75	23.91	0.40	1.87	12.75	15.04	0.54	—	11.30	15.67	16.96	24.10	9.07	nd	11.24	1.41
U251	—	—	—	0.78	5.21	—	—	—	5.29	3.11	27.61	23.51	23.39	5.12	4.94
Melanoma															
LOX IMVIL	13.08	6.16	2.80	6.09	nd	1.01	—	8.81	—	nd	19.88	2.64	51.38	1.03	6.44
MALME-3M	3.60	4.11	—	6.47	—	0.52	—	6.43	1.19	4.28	9.94	15.60	nd	2.51	—
M14	6.96	—	—	1.40	—	—	—	5.31	—	—	—	6.20	39.09	1.20	—
MDA-MB-435	5.47	—	—	1.21	—	—	—	—	—	—	8.04	1.69	89.75	9.40	2.65
SK-MEL-2	—	—	—	4.74	—	—	—	—	0.22	—	—	0.66	21.17	—	—
SK-MEL-28	3.13	3.73	6.94	—	—	—	—	—	—	—	8.53	6.26	19.54	—	—
SK-MEL-5	12.63	4.51	4.22	1.58	—	2.10	—	6.39	5.73	0.36	23.53	14.42	58.49	7.56	3.64
UACC-257	10.51	—	6.70	4.44	11.51	0.88	—	10.88	—	9.84	6.74	1.17	13.91	2.77	—
UACC-62	24.94	16.32	nd	11.89	4.96	nd	4.25	6.82	5.82	3.64	nd	12.21	40.93	nd	nd
Ovarian cancer															
IGROV1	—	2.59	—	—	—	—	—	—	—	—	—	—	nd	—	—
OVCAR-3	—	—	—	—	—	—	—	—	—	—	2.26	—	61.37	1.40	—
OVCAR-4	3.78	—	—	—	—	—	5.64	—	—	0.93	0.90	4.52	18.02	—	—
OVCAR-5	—	—	—	0.02	—	—	—	—	—	3.24	6.42	—	—	4.29	—
OVCAR-8	1.22	—	—	0.27	—	—	—	0.54	1.76	1.10	10.05	9.38	20.59	—	—
NCI/ADR-RES	3.78	—	—	—	—	—	—	3.20	—	—	—	6.74	15.77	—	—
SK-OV-3	13.01	5.76	—	—	5.23	—	—	17.39	—	6.07	—	—	19.85	—	—
Renal cancer															
786-0	2.21	15.91	—	—	—	—	—	—	—	—	33.50	23.26	28.18	0.15	4.55
A498	—	23.81	—	—	5.65	—	—	—	—	9.02	—	—	—	—	—
ACHN	3.57	0.66	—	0.08	—	—	—	—	—	—	5.56	—	14.44	0.56	—

Table 3 (*Contd.*)

Cell line	GI%														
	8a	8b	8c	8d	8e	8f	8g	8h	8i	8j	8k	8l	8m	8n	8o
CAKI-1	14.61	7.21	1.61	11.95	12.53	—	—	8.60	16.73	10.33	2.24	—	46.89	4.01	—
RXF 393	2.39	35.48	3.30	—	—	—	—	11.61	—	—	56.78	20.04	60.70	—	8.94
SN12C	nd	4.88	—	nd	—	—	—	nd	nd	11.01	3.15	3.47	2.96	0.98	—
TK-10	—	—	—	—	—	—	—	—	—	4.82	—	—	—	—	—
UO-31	12.64	17.10	—	6.47	11.83	0.65	7.75	6.90	8.39	14.38	—	4.31	nd	11.97	—
Prostate cancer															
PC-3	6.14	—	5.34	3.02	—	4.74	—	6.70	—	—	7.42	1.90	32.87	7.50	1.89
DU-145	—	—	—	—	—	—	—	—	—	—	6.11	6.23	3.98	—	—
Breast cancer															
MCF7	29.97	12.29	10.13	13.97	3.73	18.37	6.70	10.92	13.11	4.45	17.44	13.20	72.06	11.26	20.18
MDA-MB-231/ATCC	16.75	2.75	—	7.21	nd	—	—	6.65	9.78	nd	—	—	—	—	—
HS 578T	11.91	8.98	—	—	nd	—	0.37	—	1.76	nd	38.46	6.10	42.19	12.33	3.82
BT-549	10.35	—	—	—	—	—	—	—	—	—	41.45	15.93	39.33	1.30	—
T-47D	12.15	15.55	nd	—	—	nd	1.54	2.11	5.26	8.11	nd	17.60	28.76	nd	nd
MDA-MB-468	1.73	—	—	—	5.40	—	—	4.23	—	2.65	—	—	69.10	—	—
Mean GI%	6.25	1.04	—	0.81	—	—	—	1.91	—	1.78	8.39	6.72	31.21	1.42	—

[a] Showed no GI%. [b] Not detected.

Table 4 Cytotoxic activity of **8m** on MCF-7 cell line

Compound ID	[a]IC_{50} (μM)
8m	5.03 ± 0.43
Sorafenib	3.24 ± 0.21

[a] IC_{50} are mean of 3 independent experiments $\pm$ SD.

Table 5 Effect of **8m** on the different phases MCF7 cell line

Comp	% G0/G1	% S	% G2/M	% Sub-G1
Control	57.89	23.88	18.23	1.63
8m	51.04	23.70	25.26	2.08

cells rose from 0.09% and 0.42% in control cells to 5.24% and 31.23%, respectively, following treatment with **8m** (Fig. 5).

2.2.2.5 Wound healing assay. Compound **8m**'s impact on the migration of MCF-7 cells at 5 μM (IC_{50} concentration) was tested by the employment of wound healing assay. In this experiment, untreated cells and **8m**-treated cells were both examined regularly after making horizontal scratches into the confluent monolayer. Fig. 6 was used to display the results. A delay in the scratch closer following treatment with **8m** was observed as
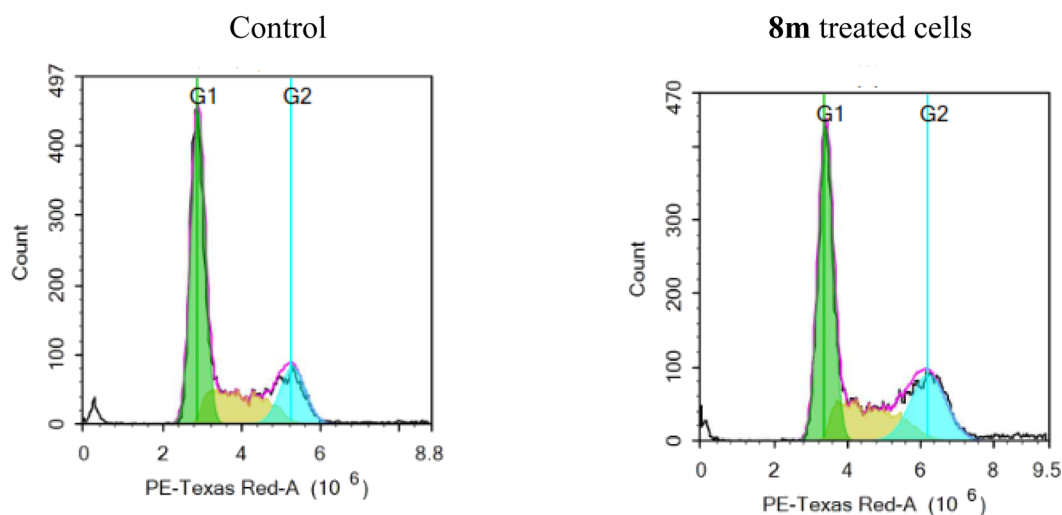
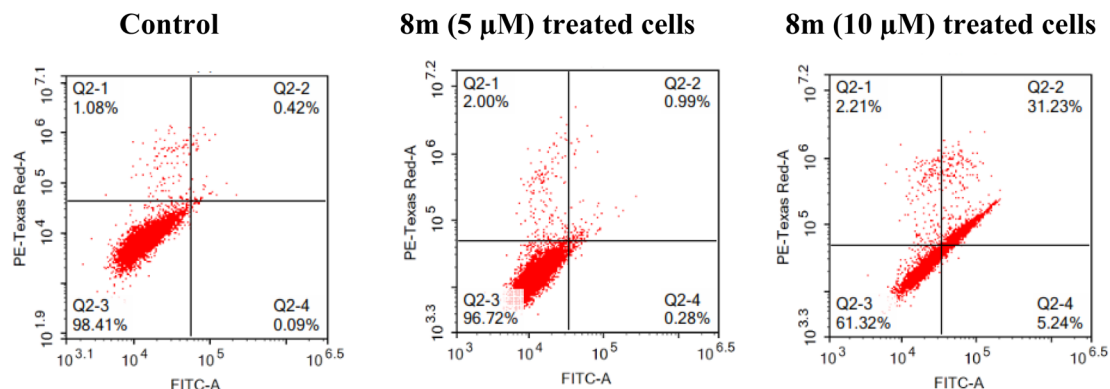**Fig. 4** Compound **8m**'s effect on MCF-7 cells' cell cycle stages.

Fig. 5 Effect of **8m** on the percentage of annexin V-FITC-positive staining in MCF-7 cell line, the four quadrants are: **Q2-1** (necrotic), **Q2-2** (late apoptotic), **Q2-3** (viable); **Q2-4** (early apoptotic).

evidenced by a distance of 0.71, 0.57 and 0.46 mm in **8m** treated cells in comparison to 0.56, 0.39 and 0.22 mm in control cells after 24 h, 48 h and 72 h, respectively. This result highlights how treatment with **8m** altered the migration of MCF-7 cells in comparison to control cells which supports the anti-migratory properties of **8m**.

2.3. Molecular docking simulation

Employing Autodock Vina,[31] the benzimidazole–dioxo(benzo) isoindoline conjugates **8c** and **8m** were docked in the binding sites' of VEGFR-2 (PDB ID: 4ASD)[34] and FGFR-1 (PDB ID: 4V01).[35] In order to visualise the findings of the docking experiments,

a free BIOVIA Discovery Studio Visualizer was utilised (**https://discover.3ds.com/discovery-studio-visualizer-download**). The co-crystallized ligand was self-docked to verify the validation of the docking methods.[36]

The validation experiment displayed that the docked poses are superimposed on the co-crystalized ligands and have the ability to reproduce all the binding interactions with the key amino acids with docking energy scores of -12.20 and -13.40 kcal mol^{-1} in VEGFR-2 and FGFR-1, respectively (For further details see ESI†). Docking of **8c** and **8m** demonstrated binding energy scores of -10.10 and -10.70 kcal mol^{-1}, respectively on VEGFR-2 binding energy scores of -9.2 and -9.51 kcal mol^{-1}, respectively on FGFR-1.
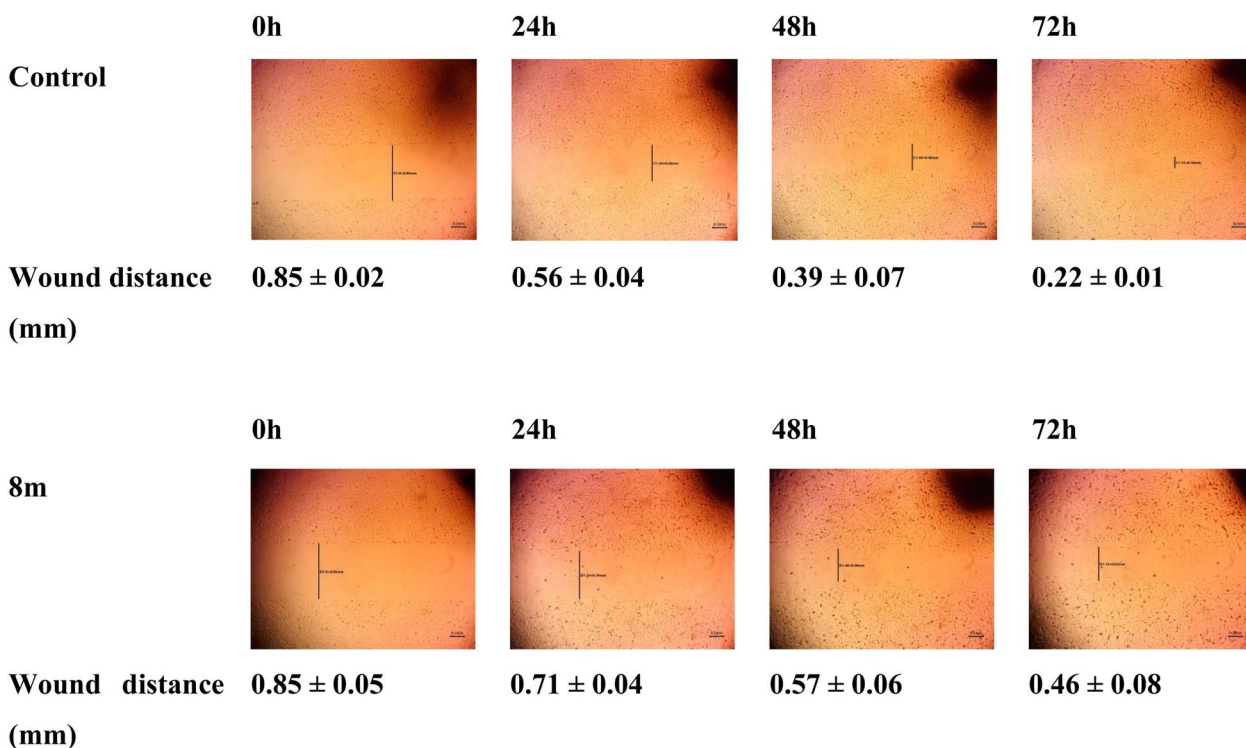
Fig. 6 Daily measurement of the wound distances of MCF-7 cell line before and after treatment with **8m**.
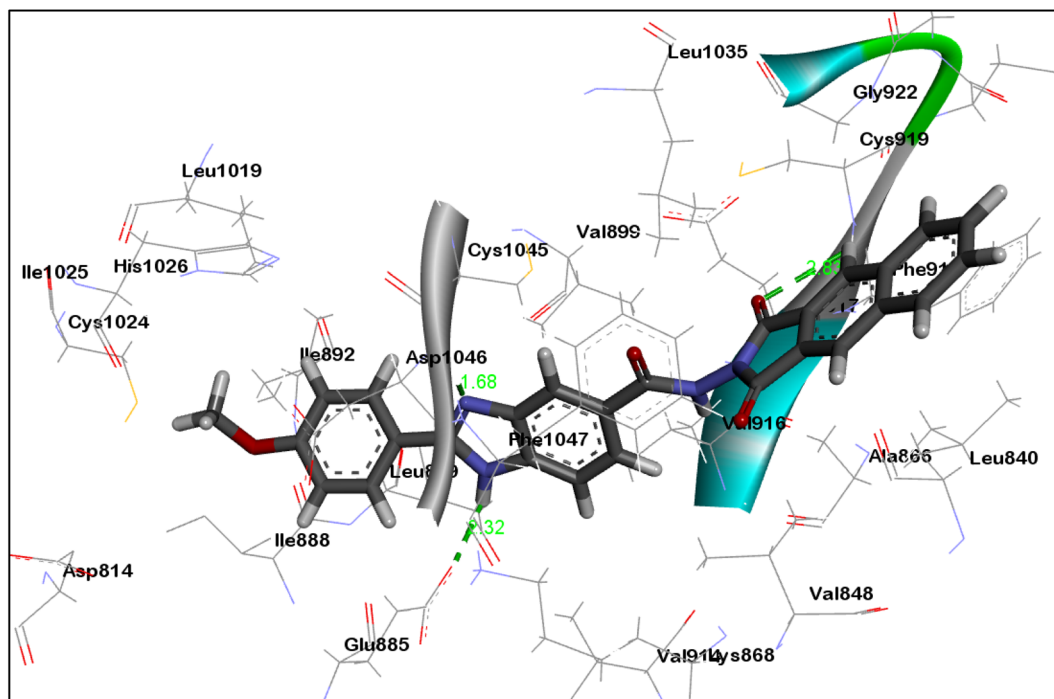
Fig. 7 3D presentation of **8m** in the binding site of VEGFR-2.

As can be seen in Fig. 7 and 8, the dioxobenzoisoindoline moiety is positioned in the ATP binding site where one CO group establish hydrogen bonding with the essential amino acids Cys919 and Ala564 in the VEGFR-2's and FGFR-1's binding sites, respectively. Additionally, the dioxobenzoisoindoline moiety is involved in hydrophobic interactions with Leu840,
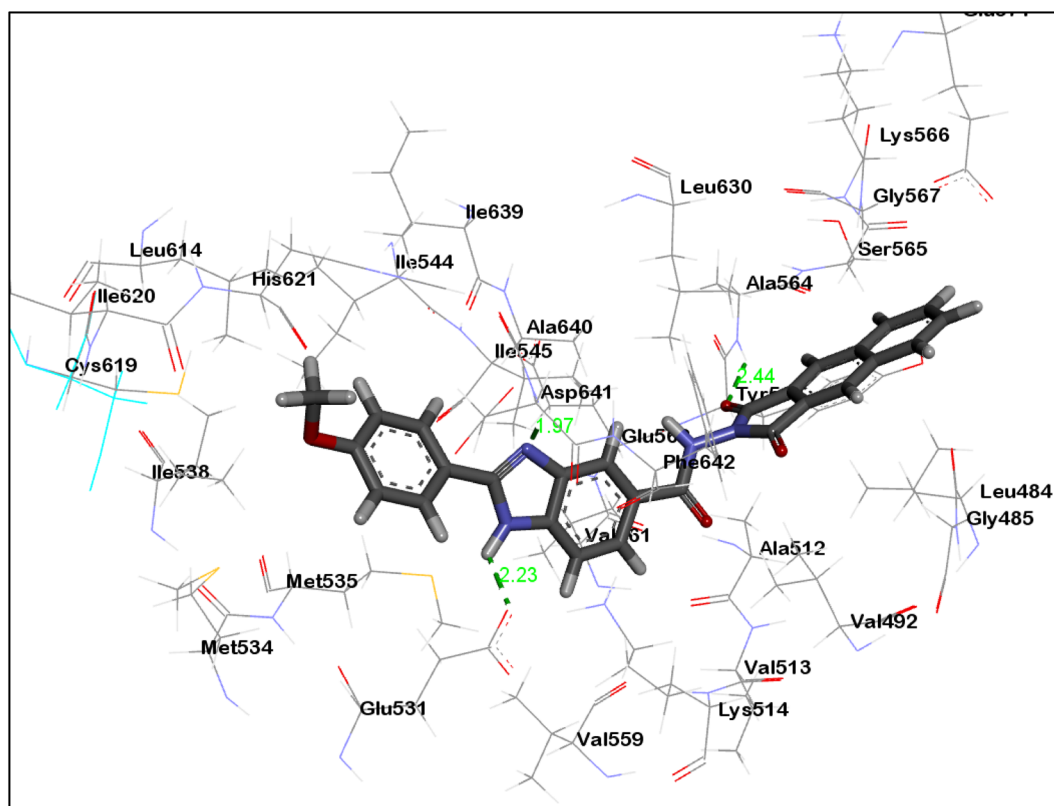

Fig. 8 3D presentation of **8m** in the binding site of FGFR-1.

Table 6 Physicochemical and AMDE properties prediction of **8a–o** using SwissADME

Compound ID	MW	#Rotatable bonds	#H-bond acceptors	#H-bond donors	MR	TPSA	iLOGP	GI absorption	BBB permeant	Pgp substrate	Lipinski #violations	Bioavailability score	Synthetic accessibility
8a	416.82	4	4	2	114.53	95.16	2.16	High	No	No	0	0.55	2.62
8b	412.4	5	5	2	116.01	104.39	2.27	High	No	No	0	0.55	2.72
8c	412.4	5	5	2	116.01	104.39	2.14	High	No	No	0	0.55	2.7
8d	442.42	6	6	2	122.5	113.62	2.75	High	No	Yes	0	0.55	2.92
8e	472.45	7	7	2	128.99	122.85	2.62	High	No	Yes	0	0.55	3.1
8f	460.83	5	6	3	121.49	132.46	1.46	High	No	No	0	0.55	2.82
8g	456.41	6	7	3	122.97	141.69	1.75	Low	No	No	0	0.55	2.94
8h	456.41	6	7	3	122.97	141.69	1.65	Low	No	No	0	0.55	2.91
8i	486.43	7	8	3	129.46	150.92	1.7	Low	No	No	1	0.55	3.13
8j	516.46	8	9	3	135.95	160.15	2.1	Low	No	Yes	2	0.17	3.31
8k	466.88	4	4	2	132.03	95.16	2.6	High	No	No	0	0.55	2.85
8l	462.46	5	5	2	133.52	104.39	2.62	High	No	No	0	0.55	2.95
8m	462.46	5	5	2	133.52	104.39	2.46	High	No	No	0	0.55	2.93
8n	492.48	6	6	2	140.01	113.62	3.02	High	No	Yes	0	0.55	3.15
8o	522.51	7	7	2	146.5	122.85	3.01	High	No	Yes	1	0.55	3.34

Val848, Ala866, Phe918, Cys919 and Leu1035 in VEGFR-2 and Leu484, Val492, Ala512 and Leu630 in FGFR-1.

The benzimidazole moiety is positioned at the interface between the gate area and hydrophobic pocket forming through the NH group of the benzimidazole moiety hydrogen bonding with Glu885 and Glu531 residues in VEGFR-2 and FGFR-1, respectively. Simultaneously, the C=N group forms hydrogen bonding with Asp1046 and Asp641 residues of VEGFR-2 and FGFR-1, respectively. Moreover, the benzimidazole core creates hydrophobic interactions with the amino acids Lys868, Leu889, Val899, Val916 and Cys1045 in the gate area of VEGFR-2 as well as with the amino acids Lys514, Met535, Ile545, Val561, Leu614 and Ala640 in FGFR-1.

The 4-methoxyphenyl group at the 2-position of the benzimidazole scaffold is settled in the hydrophobic pocket creating hydrophobic interactions with the amino acids Ile888, Leu889 and Ile892 in VEGFR-2 and Cys619 and His621 in FEGR-1 (Fig. 7 and 8).

2.4. ADME properties prediction

In order to analyze the drug-likeness of the designed and synthesized benzimidazole-dioxo(benzo)isoindoline conjugates **8a–o**, they were submitted to free SwissADME webtool and certain findings were chosen to be displayed in Table 6.[32] The information received showed that the majority of the hybrids presented meet Lipinski's rule of 5.[37] The conjugates **8i**, **8j** and **8o** are the only exceptions. The conjugates **8a–f** and **8k–o** are anticipated to be well absorbed from GIT.[38] At the meantime, none of the candidates **8a–o** are expected to cross the blood–brain barrier, demonstrating that the central nervous system won't be affected. The synthesized candidates show reasonable bioavailability scores and synthetic viability.[39] In addition, the bioavailability radar chart of the synthesized candidate (see ESI,† and Fig. 9) proved that **8a–o** exhibit ideal size, lipophilicity, polarity, flexibility and solubility for oral bioavailability. The only characteristic that deviates slightly from its ideal value is the degree of saturation.
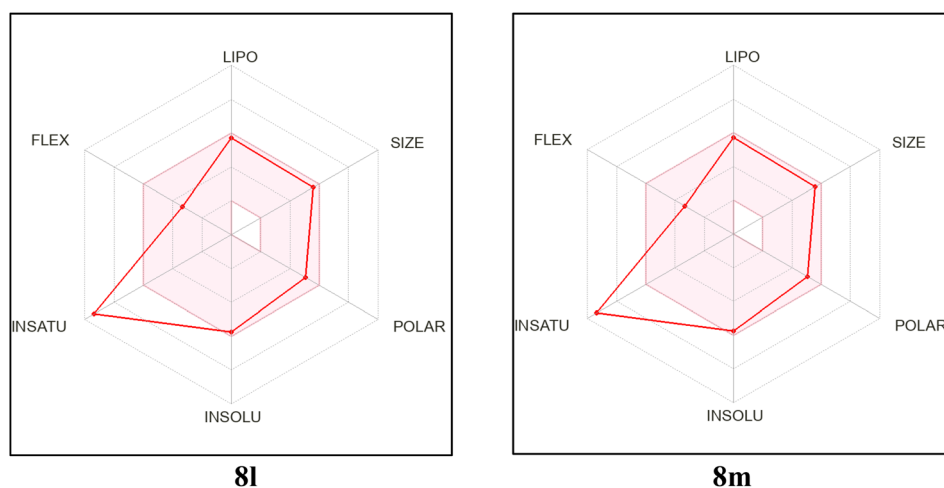

8l

8m

Fig. 9 Bioavailability radar chart from SwissADME free web tool of **8l** and **8m**.

3. Conclusion

In this study, a new series of benzimidazole–dioxo(benzo)iso-indoline hybrids 8a–o were rationally constructed and synthesized. We examined the VEGFR-2 inhibitory activity of each synthesized hit at a dose of 10 μM. Potent inhibitory activity was observed by the conjugates 8l and 8m with % inhibition = 87.61% and 80.69%, respectively. Additionally, 8l and 8m revealed potent FGFR-1 inhibition % of 84.20% and 76.83%. Examining the target hits' growth inhibitory effectiveness on NCI cancer cell lines revealed that the most effective hybrid is 8m. It demonstrated growth inhibition % up to 89.75%. Further studies proved that 8m caused G2/M phase cell cycle arrest and potentiated the apoptosis of MCF7 cell line. Furthermore, 8m demonstrated strong antimigratory properties, as evidenced by the delayed wound closure compared to untreated cells. Furthermore, the ability of benzimidazole–dioxobenzoisoindoline hybrid 8m to occupy the binding sites of VEGFR-2 and FGFR-1 and perform the necessary interactions with the crucial amino acids in those binding pockets was demonstrated by molecular docking simulations. Additionally, ADME prediction studies showed that the target benzimidazole–dioxoisoindoline hybrids 8a–o may had desired drug-like properties.

4. Experimental

4.1. Chemistry

4.1.1. General remarks. Chemical companies provided the solvents and chemicals that were used, without further purifications in chemical synthesis of target benzimidazole–dioxoisoindolines 8a–o. Precoated silica gel 60 F245 aluminium plates (Merck) were used to track the reaction's development. Target products 8a–o were purified by crystallization from methanol. The melting points were recorded using a Stuart SMP30 melting point device. The ^{1}H NMR and ^{13}C NMR (DMSO-d_6) spectra were acquired using Bruker AM500 at 500/125 MHz and using Bruker AM400 at 400/100 MHz. Chemical shifts are reported in δ (parts per million: ppm) using TMS as internal standard. Solvent peak was referenced to (2.50 ppm for ^{1}H NMR and 39.500 ppm for ^{13}C NMR). Splitting of signals in ^{1}H NMR was described as follows: br. (broad), s (singlet), d (doublet), t (triplet), dd (doublet of doublets), m (multiplet), Coupling constants (J) were recorded directly from the spectra and represented in Hertz (Hz). High resolution mass spectra were recorded on Agilent 6200 Series TOF and 6500 Series Q-TOF instrument.

4.1.2. Synthesis of starting benzimidazoles 4a–e, 5a–e and 6a–e. Following previously published procedures,[19,20] the 2-substituted benzimidazole-5-carboxylic acids 4a–e, 5-ethyl esters 5a–e, and 5-carbohydrazides 6a–e were prepared.

4.1.3. Synthesis of benzimidazole–dioxoisoindoles 8a–o. Benzimidazole-5-carbohydrazides 6a–e and acid anhydrides 7a–c were interacted in glacial acetic acid under reflux for 3 h. The precipitate was collected and purified by recrystallized from methanol to provide the desired benzimidazole–dioxoisoindolines 8a–o.

4.1.3.1 2-(4-Chlorophenyl)-N-(1,3-dioxoisoindolin-2-yl)-1H-benzo[d]imidazole-5-carboxamide (8a). Yield = 51%; mp > 300 °C; ^{1}H NMR (400 MHz; DMSO-d_6) δ$_H$ 7.68 (d, ^3J = 8.4 Hz, 2H), 7.88 (d like, ^3J = 8.4 Hz, 1H) 7.97–8.05 (m, 4H), 8.19 (br., 1H), 8.24 (d, ^3J = 8.4 Hz, 2H), 8.37 (br., 1H), 11.30 (s, 1H), 13.38 ppm (br., 1H); ^{13}C NMR (100 MHz; DMSO-d_6) δ$_C$ 112.18, 119.51, 124.34, 128.87, 128.99, 129.68, 129.98, 135.67, 135.91, 166.06, 166.23 ppm; anal. calcd for $C_{22}H_{13}ClN_4O_3$: C, 63.39; H, 3.14; N, 13.44; found: C, 63.56; H, 3.27; N, 13.76.

4.1.3.2 N-(1,3-dioxoisoindolin-2-yl)-2-(3-methoxyphenyl)-1H-benzo[d]imidazole-5-carboxamide (8b). Yield = 58%; mp > 300 °C; ^{1}H NMR (400 MHz; DMSO-d_6) δ$_H$ 3.88 (s, 3H), 7.12 (dd, ^3J = 8.0 Hz, ^4J = 2.0 Hz, 1H), 7.51 (t, ^3J = 8.0 Hz, 1H), 7.75–7.83 (m, 3H), 7.88 (d, ^3J = 8.0 Hz, 1H), 7.97–8.00 (m, 2H), 8.02–8.05 (m, 2H), 8.24–8.32 (m, 1H), 11.31 (s, 1H), 13.30 ppm (br., 1H); ^{13}C NMR (100 MHz; DMSO-d_6) δ$_C$ 55.37, 111.79, 116.49, 119.14, 122.47, 123.89, 124.60, 129.56, 130.28, 130.86, 135.44, 153.68, 159.71, 165.63, 165.80 ppm; anal. calcd for $C_{23}H_{16}N_4O_4$: C, 66.99; H, 3.91; N, 13.59; found: C, 66.71; H, 4.23; N, 13.32.

4.1.3.3 N-(1,3-dioxoisoindolin-2-yl)-2-(4-methoxyphenyl)-1H-benzo[d]imidazole-5-carboxamide (8c). Yield = 51%; mp > 300 °C; ^{1}H NMR (400 MHz; DMSO-d_6) δ$_H$ 3.86 (s, 3H), 7.15 (d, ^3J = 8.8 Hz, 2H), 7.71 (d, ^3J = 8.8 Hz, 1H), 7.85 (dd, ^3J = 8.4 Hz, ^4J = 1.6 Hz, 1H), 7.97–8.00 (m, 2H), 8.01–8.05 (m, 2H), 8.17 (d, ^3J = 8.8 Hz, 2H), 8.24 (br., 1H), 11.28 (s, 1H), 13.13 ppm (br., 1H); ^{13}C NMR (100 MHz; DMSO-d_6) δ$_C$ 55.43, 114.55, 121.89, 122.00, 123.89, 124.30, 128.46, 128.53, 129.58, 130.79, 132.90, 135.44, 153.90, 161.18, 165.66, 165.83, 168.72 ppm; anal. calcd for $C_{23}H_{16}N_4O_4$: C, 66.99; H, 3.91; N, 13.59; found: C, 66.70; H, 3.78; N, 13.82; HRMS (+) ESI *m/z* calculated for $C_{23}H_{17}N_4O_4$ [M + H]$^+$: 413.1250, found: 413.1236.

4.1.3.4 2-(2,5-Dimethoxyphenyl)-N-(1,3-dioxoisoindolin-2-yl)-1H-benzo[d]imidazole-5-carboxamide (8d). Yield = 49%; mp > 300 °C; ^{1}H NMR (400 MHz; DMSO-d_6) δ$_H$ 3.82 (s, 3H), 4.00 (s, 3H), 7.11 (dd, ^3J = 8.8 Hz, ^4J = 3.2 Hz, 1H), 7.22 (d, ^3J = 9.2 Hz, 1H), 7.79 (d, ^3J = 8.4 Hz, 1H), 7.87 (dd, ^3J = 8.4 Hz, ^4J = 1.2 Hz, 1H), 7.90 (d, ^4J = 3.2 Hz, 1H), 7.97–7.99 (m, 2H), 8.02–8.04 (m, 2H), 8.33 (s, 1H), 11.28 (s, 1H), 12.74 ppm (br., 1H); ^{13}C NMR (100 MHz; DMSO-d_6) δ$_C$ 55.60, 56.24, 113.58, 113.87, 117.78, 117.92, 121.84, 123.88, 124.50, 128.53, 129.58, 130.78, 132.94, 135.43, 151.28, 151.37, 153.25, 165.63, 166.00, 168.71 ppm; anal. calcd for $C_{24}H_{18}N_4O_5$: C, 65.15; H, 4.10; N, 12.66; found: C, 65.38; H, 3.85; N, 12.89.

4.1.3.5 N-(1,3-dioxoisoindolin-2-yl)-2-(3,4,5-trimethoxyphenyl)-1H-benzo[d]imidazole-5-carboxamide (8e). Yield = 52%; mp > 300 °C; ^{1}H NMR (400 MHz; DMSO-d_6) δ$_H$ 3.76 (s, 3H), 3.93 (s, 6H), 7.57 (s, 2H), 7.76 (d, ^3J = 8.4 Hz, 1H), 7.88 (dd, ^3J = 8.4 Hz, ^4J = 1.6 Hz, 1H), 7.97–8.00 (m, 2H), 8.02–8.05 (m, 2H), 8.26 (br., 1H), 11.32 (s, 1H), 12.06 ppm (br., 1H); ^{13}C NMR (100 MHz; DMSO-d_6) δ$_C$ 56.18, 60.27, 104.33, 115.32, 122.20, 123.94, 124.58, 124.78, 129.61, 135.50, 139.53, 153.37, 153.84, 165.71, 165.86 ppm; anal. calcd for $C_{25}H_{20}N_4O_6$: C, 63.56; H, 4.27; N, 11.86; found: C, 63.78; H, 4.50; N, 11.53.

4.1.3.6 2-(2-(4-Chlorophenyl)-1H-benzo[d]imidazole-5-carboxamido)-1,3-dioxoisoindoline-5-carboxylic acid (8f). Yield = 55%; mp = 291–293 °C; ^{1}H NMR (400 MHz; DMSO-d_6) δ$_H$ 7.68 (d, ^3J = 8.4 Hz, 2H), 7.76 (d like, ^3J = 6.4 Hz, 1H), 7.88 (dd, ^3J = 8.4 Hz, ^4J = 0.8 Hz, 1H), 8.16 (d, ^3J = 7.6 Hz, 1H), 8.24 (d, ^3J = 8.8 Hz, 2H), 8.29 (br., 1H), 8.37 (s, 1H), 8.48 (dd, ^3J = 8.0 Hz, ^4J =

1.2 Hz, 1H), 11.41 (s, 1H), 13.41 ppm (br., 2H); ^{13}C NMR (100 MHz; DMSO-d_6) δ_C 123.89, 124.39, 124.60, 128.44, 128.54, 129.21, 129.95, 132.72, 135.19, 136.14, 137.13, 164.82, 164.86, 165.64, 165.71 ppm; anal. calcd for $C_{23}H_{13}ClN_4O_5$: C, 59.95; H, 2.84; N, 12.16; found: C, 59.71; H, 3.12; N, 12.00.

4.1.3.7 2-(2-(3-Methoxyphenyl)-1H-benzo[d]imidazole-5-carboxamido)-1,3-dioxoisoindoline-5-carboxylic acid (8g). Yield = 63%; mp > 300 °C; ^{1}H NMR (400 MHz; DMSO-d_6) δ_H 3.88 (s, 3H), 7.12 (dd, ^3J = 8.0 Hz, ^4J = 2.0 Hz, 1H), 7.50 (t, ^3J = 8.0 Hz, 1H), 7.77–7.82 (m, 3H), 7.89 (d, ^3J = 8.4 Hz, 1H), 8.15 (d, ^3J = 7.6 Hz, 1H), 8.30 (br., 1H), 8.38 (s, 1H), 8.48 (dd, ^3J = 8.0 Hz, ^4J = 1.2 Hz, 1H), 11.41 (s, 1H), 13.33 ppm (br., 2H); ^{13}C NMR (100 MHz; DMSO-d_6) δ_C 55.39, 111.80, 116.51, 119.16, 122.21, 123.92, 124.41, 124.51, 129.98, 130.29, 130.85, 132.73, 136.17, 137.22, 153.64, 159.72, 164.87, 164.92, 165.70, 165.81 ppm; anal. calcd for $C_{24}H_{16}N_4O_6$: C, 63.16; H, 3.53; N, 12.28; found: C, 63.35; H, 3.39; N, 12.44.

4.1.3.8 2-(2-(4-Methoxyphenyl)-1H-benzo[d]imidazole-5-carboxamido)-1,3-dioxoisoindoline-5-carboxylic acid (8h). Yield = 69%; mp > 300 °C; ^{1}H NMR (400 MHz; DMSO-d_6) δ_H 3.86 (s, 3H), 7.15 (d, ^3J = 8.8 Hz, 2H), 7.71 (d, ^3J = 8.4 Hz, 1H), 7.85 (dd, ^3J = 8.4 Hz, ^4J = 1.2 Hz, 1H), 8.15–8.18 (m, 3H), 8.24 (br., 1H), 8.37 (s, 1H), 8.48 (dd, ^3J = 8.0 Hz, ^4J = 1.2 Hz, 1H), 11.37 (s, 1H), 13.07 ppm (br., 2H); ^{13}C NMR (100 MHz; DMSO-d_6) δ_C 55.44, 114.55, 121.98, 123.93, 124.17, 124.41, 128.52, 129.99, 132.75, 136.18, 137.18, 153.97, 161.16, 164.89, 164.94, 165.70, 165.88 ppm; anal. calcd for $C_{24}H_{16}N_4O_6$: C, 63.16; H, 3.53; N, 12.28; found: C, 63.46; H, 3.81; N, 11.96.

4.1.3.9 2-(2-(2,5-Dimethoxyphenyl)-1H-benzo[d]imidazole-5-carboxamido)-1,3-dioxoisoindoline-5-carboxylic acid (8i). Yield = 65%; mp > 300 °C; ^{1}H NMR (400 MHz; DMSO-d_6) δ_H 3.82 (s, 3H), 4.00 (s, 3H), 7.11 (dd, ^3J = 8.8 Hz, ^4J = 3.2 Hz, 1H), 7.22 (d, ^3J = 9.2 Hz, 1H), 7.78 (d, ^3J = 8.4 Hz, 1H), 7.87 (dd, ^3J = 8.4 Hz, ^4J = 1.2 Hz, 1H), 7.90 (d, ^4J = 3.2 Hz, 1H), 8.15 (d, ^3J = 7.6 Hz, 1H), 8.33 (s, 1H), 8.37 (s, 1H), 8.48 (dd, ^3J = 8.0 Hz, ^4J = 1.2 Hz, 1H), 11.36 (s, 1H), 12.48 (br., 1H), 13.84 ppm (br., 1H); ^{13}C NMR (100 MHz; DMSO-d_6) δ_C 55.73, 56.35, 113.71, 113.96, 117.81, 118.11, 122.00, 124.03, 124.52, 130.08, 132.84, 136.32, 137.29, 151.50, 153.36, 164.98, 165.02, 165.85, 166.22 ppm; anal. calcd for $C_{25}H_{18}N_4O_7$: C, 61.73; H, 3.73; N, 11.52; found: C, 61.52; H, 3.98; N, 11.76.

4.1.3.10 1,3-Dioxo-2-(2-(3,4,5-trimethoxyphenyl)-1H-benzo[d]imidazole-5-carboxamido)-isoindoline-5-carboxylic acid (8j). Yield = 68%; mp > 300 °C; ^{1}H NMR (400 MHz; DMSO-d_6) δ_H 3.76 (s, 3H), 3.93 (s, 6H), 7.57 (s, 2H), 7.75 (d, ^3J = 8.4 Hz, 1H), 7.88 (dd, ^3J = 8.8 Hz, ^4J = 1.6 Hz, 1H), 8.16 (d, ^3J = 7.5 Hz, 1H), 8.26 (br., 1H), 8.38 (s, 1H), 8.49 (dd, ^3J = 7.8 Hz, ^4J = 1.2 Hz, 1H), 11.38 (s, 1H), 12.70 ppm (br., 1H); ^{13}C NMR (100 MHz; DMSO-d_6) δ_C 56.13, 60.22, 104.28, 120.36, 122.10, 123.91, 124.37, 124.39, 124.81, 129.98, 132.73, 136.14, 137.18, 139.46, 153.31, 164.89, 164.93, 165.67, 165.80 ppm; anal. calcd for $C_{26}H_{20}N_4O_8$: C, 60.47; H, 3.90; N, 10.85; found: C, 60.22; H, 3.59; N, 10.98.

4.1.3.11 2-(4-Chlorophenyl)-N-(1,3-dioxo-1,3-dihydro-2H-benzo[f]isoindol-2-yl)-1H-benzo[d]imidazole-5-carboxamide (8k). Yield = 54%; mp 220-222 °C; ^{1}H NMR (400 MHz; DMSO-d_6) δ_H 7.68 (d, ^3J = 8.4 Hz, 2H), 7.78 (d like, ^3J = 6.4 Hz, 1H), 7.93 (dd, ^3J = 7.6 Hz, ^4J = 1.6 Hz, 1H), 7.95 (t, ^3J = 7.6 Hz, 2H), 8.25 (d, ^3J = 8.8 Hz, 2H), 8.34 (br., 1H), 8.57 (d, ^3J = 8.4 Hz, 2H), 8.60 (d, ^3J = 7.2 Hz, 2H), 11.33 (s, 1H), 13.37 ppm (br., 1H); ^{13}C NMR (100 MHz; DMSO-d_6) δ_C 121.74, 125.77, 127.30, 127.57, 128.54, 128.56, 129.26, 131.62, 131.69, 135.20, 135.34, 152.61, 162.01, 165.69 ppm; anal. calcd for $C_{26}H_{15}ClN_4O_3$: C, 66.89; H, 3.24; N, 12.00; found: C, 66.64; H, 3.38; N, 12.26.

4.1.3.12 N-(1,3-dioxo-1,3-dihydro-2H-benzo[f]isoindol-2-yl)-2-(3-methoxyphenyl)-1H-benzo[d]imidazole-5-carboxamide (8l). Yield = 55%; mp 215–217 °C; ^{1}H NMR (400 MHz; DMSO-d_6) δ_H 3.89 (s, 3H), 7.12 (dd, ^3J = 8.0 Hz, ^4J = 2.0 Hz, 1H), 7.51 (t, ^3J = 8.0 Hz, 1H), 7.77–7.83 (m, 3H), 7.92–7.96 (m, 3H), 8.33 (br.,1H), 8.55 (d, ^3J = 8.0 Hz, 2H), 8.59 (d, ^3J = 7.2 Hz, 2H), 11.32 (s, 1H), 13.40 ppm (br., 1H); ^{13}C NMR (100 MHz; DMSO-d_6) δ_C 55.43, 111.81, 116.52, 119.17, 121.76, 125.66, 127.32, 127.60, 130.35, 130.93, 131.65, 131.72, 135.37, 135.48, 159.77, 162.04, 165.75 ppm; anal. calcd for $C_{27}H_{18}N_4O_4$: C, 70.12; H, 3.92; N, 12.12; found: C, 70.42; H, 3.75; N, 12.35.

4.1.3.13 N-(1,3-dioxo-1,3-dihydro-2H-benzo[f]isoindol-2-yl)-2-(4-methoxyphenyl)-1H-benzo[d]imidazole-5-carboxamide (8m). Yield = 58%; mp 208–210 °C; ^{1}H NMR (400 MHz; DMSO-d_6) δ_H 3.86 (s, 3H), 7.15 (d, ^3J = 8.8 Hz, 2H), 7.73 (br., 1H), 7.90 (t, ^3J = 7.6 Hz, 1H), 7.96 (t, ^3J = 7.6 Hz, 2H), 8.18 (d, ^3J = 8.8 Hz, 2H), 8.52–8.61 (m, 5H), 11.28 (s, 1H), 13.12 ppm (br., 1H); ^{13}C NMR (100 MHz; DMSO-d_6) δ_C 55.40, 114.49, 118.98, 121.71, 122.11, 125.19, 127.25, 127.51, 127.54, 128.42, 129.70, 131.36, 131.58, 131.62, 132.47, 135.27, 135.39, 160.71, 161.05, 161.97, 165.70 ppm; anal. calcd for $C_{27}H_{18}N_4O_4$: C, 70.12; H, 3.92; N, 12.12; found: C, 69.95; H, 4.20; N, 11.83; HRMS (+) ESI m/z calculated for $C_{27}H_{19}N_4O_4$ $[M + H]^+$: 463.1406, found: 463.1400.

4.1.3.14 2-(2,5-Dimethoxyphenyl)-N-(1,3-dioxo-1,3-dihydro-2H-benzo[f]isoindol-2-yl)-1H-benzo[d]imidazole-5-carboxamide (8n). Yield = 50%; mp 205–207 °C; ^{1}H NMR (400 MHz; DMSO-d_6) δ_H 3.83 (s, 3H), 4.01 (s, 3H), 7.11 (dd, ^3J = 8.8 Hz, ^4J = 2.8 Hz, 1H), 7.22 (d, ^3J = 9.2 Hz, 1H) 7.76–7.83 (m, 1H), 7.90–7.92 (m, 2H), 7.95 (t, ^3J = 8.0 Hz, 2H), 8.52 (d, ^3J = 6.8 Hz, 1H), 8.57 (d, ^3J = 8.0 Hz, 2H), 8.60 (d, ^3J = 8.0 Hz, 2H), 11.27 (d, J = 15.6 Hz, 1H), 12.46 ppm (d, J = 14.4 Hz, 1H); ^{13}C NMR (100 MHz; DMSO-d_6) δ_C 55.57, 56.20, 113.53, 118.96, 121.71, 127.23, 127.49, 127.52, 129.68, 131.34, 131.56, 131.60, 132.45, 134.56, 135.25, 135.38, 137.69, 142.22, 145.50, 153.21, 160.70, 161.95 ppm; anal. calcd for $C_{28}H_{20}N_4O_5$: C, 68.29; H, 4.09; N, 11.38; found: C, 68.56; H, 4.27; N, 11.66.

4.1.3.15 N-(1,3-dioxo-1,3-dihydro-2H-benzo[f]isoindol-2-yl)-2-(3,4,5-trimethoxyphenyl)-1H-benzo[d]imidazole-5-carboxamide (8o). Yield = 57%; mp 252–254 °C; ^{1}H NMR (400 MHz; DMSO-d_6) δ_H 3.76 (s, 3H), 3.93 (s, 6H), 7.58 (s, 2H), 7.77 (d, ^3J = 8.4 Hz, 1H), 7.90–7.94 (m, 3H), 8.29 (br., 1H), 8.52–8.56 (m, 4H), 11.31 (s, 1H), 13.20 ppm (br., 1H); ^{13}C NMR (100 MHz; DMSO-d_6) δ_C 56.12, 60.19, 104.24, 119.01, 121.70, 124.70, 125.52, 127.26, 127.54, 129.71, 131.36, 131.65, 132.45, 135.38, 139.43, 153.28, 160.70, 161.96, 165.56 ppm; anal. calcd for $C_{29}H_{22}N_4O_6$: C, 66.66; H, 4.24; N, 10.72; found: C, 66.39; H, 4.56; N, 11.00.

4.2. Biological activity

4.2.1. **Screening of the inhibitory activity of synthesized benzimidazole–dioxoisoindoline conjugates 8a–o on VEGFR-2.**

The synthesized 2-(substituted)-*N*-(1,3-dioxoisoindolin-2-yl)-1*H*-benzo[*d*]imidazole-5-carboxamide **8a–o** were examined for their inhibitory activity on VEGFR-2 and FGFR-1 employing assay kits purchased from BPS Biosciences – San Diego – CA – US according to the protocol provided by the manufacturer (For further details check the ESI†).[36]

4.2.2. Cell cycle analysis, apoptosis and wound healing assays. Following treatment with the benzimidazole–dioxo-benzoisoindoline conjugate **8m**, the MCF7 cell line was subjected to the previously described protocol, allowing for the identification of cell distribution at each step of the cell cycle[40] (see ESI† for further information). In the meantime, populations of necrotic and apoptotic cells were identified using a two-fluorescence channel flow cytometer and the Annexin V-FITC apoptosis detection kit (Abcam Inc., Cambridge, UK) (see ESI† for further information).[41] Procedure followed for the effect of **8m** on the wound healing was depicted in the ESI.†

4.3. Molecular modeling

Molecular docking simulations were achieved utilizing Autodock Vina[31] (For further information see ESI†). A free BIOVIA Discovery Studio Visualizer was utilised (**https://discover.3ds.com/discovery-studio-visualizer-download**) to visualize the findings.

4.4. ADME prediction studies

The SMILES notations of the target benzimidazole–dioxoisoindoline conjugates **8a–o** were submitted to SwissADME web tool to predict their physicochemical and drug likeness properties.[32]

Data availability

All data are available on request.

Conflicts of interest

The authors have no conflict of interest to declare.

Acknowledgements

References

1 R. L. Siegel, A. N. Giaquinto and A. Jemal, *Ca-Cancer J. Clin.*, 2024, **74**, 12–49.

2 H. T. Abdel-Mohsen, A. Petreni and C. T. Supuran, *Arch. Pharm.*, 2022, **355**, e2200274.

3 R. M. Hassan, W. H. Abd-Allah, A. M. Salman, A. A. El-Azzouny and M. N. Aboul-Enein, *Eur. J. Pharm. Sci.*, 2019, **139**, 105045.

4 C. Braicu, M. Buse, C. Busuioc, R. Drula, D. Gulei, L. Raduly, A. Rusu, A. Irimie, A. G. Atanasov, O. Slaby, C. Ionescu and I. Berindan-Neagoe, *Cancers*, 2019, **11**, 1618.

5 M. S. Abdel-Maksoud, A. A. B. Mohamed, R. M. Hassan, M. A. Abdelgawad, G. Chilingaryan, S. Selim, M. S. Abdel-Bakky and M. M. Al-Sanea, *Int. J. Mol. Sci.*, 2021, **22**, 10491.

6 H. T. Abdel-Mohsen, M. M. Anwar, N. S. Ahmed, S. S. Abd El-Karim and S. H. Abdelwahed, *Molecules*, 2024, **29**, 875.

7 H. T. Abdel-Mohsen, A. M. Nageeb and I. A. Y. Ghannam, *Drug Dev. Res.*, 2024, **85**, e22249.

8 R. M. Hassan, I. H. Ali, A. M. El Kerdawy, M. T. Abo-Elfadl and I. A. Y. Ghannam, *Bioorg. Chem.*, 2024, **152**, 107728.

9 K. Wada, J. Y. Lee, H. Y. Hung, Q. Shi, L. Lin, Y. Zhao, M. Goto, P. C. Yang, S. C. Kuo, H. W. Chen and K. H. Lee, *Bioorg. Med. Chem.*, 2015, **23**, 1507–1514.

10 R. H. Adams and K. Alitalo, *Nat. Rev. Mol. Cell Biol.*, 2007, **8**, 464–478.

11 C. S. Abhinand, R. Raju, S. J. Soumya, P. S. Arya and P. R. Sudhakaran, *J. Cell Commun. Signaling*, 2016, **10**, 347–354.

12 S. J. Modi and V. M. Kulkarni, *Med. Drug Discovery*, 2019, **2**, 100009.

13 D. J. Hicklin and L. M. Ellis, *J. Clin. Oncol.*, 2005, **23**, 1011–1027.

14 J. Muto, K. Shirabe, K. Sugimachi and Y. Maehara, *Hepatol. Res.*, 2015, **45**, 1–9.

15 S. Dai, Z. Zhou, Z. Chen, G. Xu and Y. Chen, *Cells*, 2019, **8**, 614.

16 M. A. Krook, J. W. Reeser, G. Ernst, H. Barker, M. Wilberding, G. Li, H. Z. Chen and S. Roychowdhury, *Br. J. Cancer*, 2021, **124**, 880–892.

17 S. S. Abd El-Karim, Y. M. Syam, A. M. El Kerdawy and H. T. Abdel-Mohsen, *Bioorg. Chem.*, 2024, **142**, 106920.

18 H. T. Abdel-Mohsen, E. A. Abd El-Meguid, A. M. El Kerdawy, A. E. E. Mahmoud and M. M. Ali, *Arch. Pharm.*, 2020, **353**, e1900340.

19 H. T. Abdel-Mohsen, M. A. Ibrahim, A. M. Nageeb and A. M. El Kerdawy, *BMC Chem.*, 2024, **18**, 42.

20 R. M. Allam, A. M. El Kerdawy, A. E. Gouda, K. A. Ahmed and H. T. Abdel-Mohsen, *Bioorg. Chem.*, 2024, **146**, 107243.

21 H. I. El Diwani, H. T. Abdel-Mohsen, I. Salama, F. A. Ragab, M. M. Ramla, S. A. Galal, M. M. Abdalla, A. Abdel-Wahab and M. A. El Demellawy, *Chem. Pharm. Bull.*, 2014, **62**, 856–866.

22 I. H. Ali, H. T. Abdel-Mohsen, M. M. Mounier, M. T. Abo-elfadl, A. M. El Kerdawy and I. A. Y. Ghannam, *Bioorg. Chem.*, 2022, **126**, 105883.

23 H. T. Abdel-Mohsen and A. El Kerdawy, *Egypt. J. Chem.*, 2024, **67**, 437–446.

24 H. T. Abdel-Mohsen, Y. M. Syam, M. S. Abd El-Ghany and S. S. Abd El-Karim, *Arch. Pharm.*, 2024, e2300721, DOI: **10.1002/ardp.202300721**.

25 M. H. Potashman, J. Bready, A. Coxon, T. M. DeMelfi Jr, L. DiPietro, N. Doerr, D. Elbaum, J. Estrada, P. Gallant, J. Germain, Y. Gu, J. C. Harmange, S. A. Kaufman,

R. Kendall, J. L. Kim, G. N. Kumar, A. M. Long, S. Neervannan, V. F. Patel, A. Polverino, P. Rose, S. Plas, D. Whittington, R. Zanon and H. Zhao, *J. Med. Chem.*, 2007, **50**, 4351–4373.

26 M. Hasegawa, N. Nishigaki, Y. Washio, K. Kano, P. A. Harris, H. Sato, I. Mori, R. I. West, M. Shibahara, H. Toyoda, L. Wang, R. T. Nolte, J. M. Veal and M. Cheung, *J. Med. Chem.*, 2007, **50**, 4453–4470.

27 R. J. Motzer, C. Porta, N. J. Vogelzang, C. N. Sternberg, C. Szczylik, J. Zolnierek, C. Kollmannsberger, S. Y. Rha, G. A. Bjarnason, B. Melichar, U. De Giorgi, V. Grünwald, I. D. Davis, J. L. Lee, E. Esteban, G. Urbanowitz, C. Cai, M. Squires, M. Marker, M. M. Shi and B. Escudier, *Lancet Oncol.*, 2014, **15**, 286–296.

28 R. Porta, R. Borea, A. Coelho, S. Khan, A. Araújo, P. Reclusa, T. Franchina, N. Van Der Steen, P. Van Dam, J. Ferri, R. Sirera, A. Naing, D. Hong and C. Rolfo, *Crit Rev Oncol Hematol*, 2017, **113**, 256–267.

29 T. D. Bunney, S. Wan, N. Thiyagarajan, L. Sutto, S. V. Williams, P. Ashford, H. Koss, M. A. Knowles, F. L. Gervasio, P. V. Coveney and M. Katan, *EBioMedicine*, 2015, **2**, 194–204.

30 T. E. Williams, S. Subramanian, J. Verhagen, C. M. McBride, A. Costales, L. Sung, W. Antonios-McCrea, M. McKenna, A. K. Louie, S. Ramurthy, B. Levine, C. M. Shafer, T. Machajewski, P. A. Renhowe, B. A. Appleton, P. Amiri,

J. Chou, D. Stuart, K. Aardalen and D. Poon, *ACS Med. Chem. Lett.*, 2015, **6**, 961–965.

31 O. Trott and A. J. Olson, *J. Comput. Chem.*, 2010, **31**, 455–461.

32 A. Daina, O. Michielin and V. Zoete, *Sci. Rep.*, 2017, **7**, 42717.

33 P. Skehan, R. Storeng, D. Scudiero, A. Monks, J. McMahon, D. Vistica, J. T. Warren, H. Bokesch, S. Kenney and M. R. Boyd, *J. Natl. Cancer Inst.*, 1990, **82**, 1107–1112.

34 M. McTigue, B. W. Murray, J. H. Chen, Y. L. Deng, J. Solowiej and R. S. Kania, *Proc. Natl. Acad. Sci. U. S. A.*, 2012, **109**, 18281–18289.

35 J. A. Tucker, T. Klein, J. Breed, A. L. Breeze, R. Overman, C. Phillips and R. A. Norman, *Structure*, 2014, **22**, 1764–1774.

36 Y. M. Syam, S. S. Abd El-Karim and H. T. Abdel-Mohsen, *Arch. Pharm.*, 2024, e2300682, DOI: **10.1002/ardp.202300682**.

37 C. A. Lipinski, F. Lombardo, B. W. Dominy and P. J. Feeney, *Adv. Drug Delivery Rev.*, 2001, **46**, 3–26.

38 W. J. Egan, K. M. Merz Jr and J. J. Baldwin, *J. Med. Chem.*, 2000, **43**, 3867–3877.

39 D. F. Veber, S. R. Johnson, H. Y. Cheng, B. R. Smith, K. W. Ward and K. D. Kopple, *J. Med. Chem.*, 2002, **45**, 2615–2623.

40 H. T. Abdel-Mohsen, M. A. Omar, A. Petreni and C. T. Supuran, *Arch. Pharm.*, 2022, **355**, e2200180.

41 H. T. Abdel-Mohsen, A. M. El Kerdawy, M. A. Omar, A. Petreni, R. M. Allam, H. I. El Diwani and C. T. Supuran, *Eur. J. Med. Chem.*, 2022, **228**, 114004.